

**Near-dissociation states and coupled potential curves for the HeN + complex**

Pavel Soldán and Jeremy M. Hutson

Citation: *The Journal of Chemical Physics* **117**, 3109 (2002); doi: 10.1063/1.1493176

View online: <http://dx.doi.org/10.1063/1.1493176>

View Table of Contents: <http://scitation.aip.org/content/aip/journal/jcp/117/7?ver=pdfcov>

Published by the [AIP Publishing](#)

---

**Articles you may be interested in**

[The Na + – H<sub>2</sub> cation complex: Rotationally resolved infrared spectrum, potential energy surface, and rovibrational calculations](#)

*J. Chem. Phys.* **129**, 184306 (2008); 10.1063/1.3005785

[Theoretical study of the He–HF + complex. II. Rovibronic states from coupled diabatic potential energy surfaces](#)

*J. Chem. Phys.* **120**, 103 (2004); 10.1063/1.1629672

[Energy levels of HCN + and DCN + in the vibronically coupled X<sup>2</sup>Π and A<sup>2</sup>Σ<sup>+</sup> states](#)

*J. Chem. Phys.* **115**, 11200 (2001); 10.1063/1.1414347

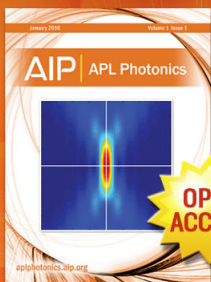
[The potential energy surface and near-dissociation states of He–H<sub>2</sub> +](#)

*J. Chem. Phys.* **110**, 3418 (1999); 10.1063/1.478208

[Contributions of the two conformers to the microwave spectrum and scattering cross-section of the He–Cl<sub>2</sub> van der Waals system, evaluated from an ab initio potential energy surface](#)

*J. Chem. Phys.* **108**, 9301 (1998); 10.1063/1.476419

---



Launching in 2016!

The future of applied photonics research is here

OPEN  
ACCESS

**AIP** | APL  
Photonics

# Near-dissociation states and coupled potential curves for the HeN<sup>+</sup> complex

Pavel Soldán<sup>a)</sup> and Jeremy M. Hutson<sup>b)</sup>

Department of Chemistry, University of Durham, South Road, Durham DH1 3LE, England

(Received 1 April 2002; accepted 21 May 2002)

The near-dissociation microwave rovibronic spectra of HeN<sup>+</sup> [Carrington *et al.*, Chem. Phys. Lett. **262**, 598 (1996)] are used to obtain coupled potential energy curves for the six electronic states correlating with He+N<sup>+</sup> <sup>3</sup>P<sub>0</sub>, <sup>3</sup>P<sub>1</sub>, and <sup>3</sup>P<sub>2</sub>. High-quality *ab initio* calculations are carried out, using a spin-restricted open-shell coupled-cluster method with an augmented correlation-consistent quintuple-zeta basis set (aug-cc-pV5Z). Fully coupled calculations of bound and quasibound states are performed, including all six electronic states, and suggest two possible assignments of the observed transitions. The potentials are then morphed (scaled) to reproduce the experimental frequencies. One of the two assignments, designated SH1, is preferred because it gives a more satisfactory explanation of the observed hyperfine splittings. The corresponding morphed potential has well depths of 1954 cm<sup>-1</sup> and 192 cm<sup>-1</sup> for the spin-free <sup>3</sup>Σ<sup>-</sup> and <sup>3</sup>Π curves, respectively.

© 2002 American Institute of Physics. [DOI: 10.1063/1.1493176]

## I. INTRODUCTION

The spectra of simple molecular ions can provide detailed information on ion-neutral interactions, which is of value in many areas of physics and chemistry. The spectra of long-range states are particularly interesting, because they also provide information on how quantum numbers and energy level patterns behave near dissociation limits, where the Born–Oppenheimer approximation is unreliable and nonadiabatic couplings play an important role. The analogous long-range states of neutral molecules have become particularly topical recently, because of interest in photoassociation spectroscopy<sup>1</sup> and the production of ultracold molecules in laser-cooled gases and Bose–Einstein condensates.<sup>2</sup>

In previous work, the spectra of near-dissociation states of HeAr<sup>+</sup> (Ref. 3), HeKr<sup>+</sup> (Ref. 4), and Ne<sub>2</sub><sup>+</sup> (Ref. 5) have been observed. The spectra were then used to determine complete sets of potential energy curves, and the couplings between them, for levels correlating with the <sup>2</sup>P<sub>3/2</sub> and <sup>2</sup>P<sub>1/2</sub> states of the atomic halogen cations. For HeAr<sup>+</sup> and Ne<sub>2</sub><sup>+</sup>, the levels were found to be described by a coupling scheme close to Hund's case (c), with quantum numbers *L* (atomic orbital angular momentum), *S* (atomic spin angular momentum), *J<sub>a</sub>* (atomic total angular momentum), *J* (total angular momentum including end-over-end rotation), and *Ω* (the projection of *J* and *J<sub>a</sub>* onto the internuclear axis). Even for HeAr<sup>+</sup>, however, the rotational couplings between states of different *Ω* are strong, so that *Ω* is not a good quantum number. For HeKr<sup>+</sup>, because of an accidental near-degeneracy between vibrational states for different values of *Ω*, this effect occurs in an extreme form. The result is that HeKr<sup>+</sup> exhibits almost pure case (e), in which *Ω* is replaced

by *R*, the space-fixed rotational angular momentum of the diatomic molecule. In case (e), there are no quantum numbers at all that describe projections onto the internuclear axis.

The purpose of the present paper is to extend this work to HeN<sup>+</sup>, for which near-dissociation spectra have also been observed by Carrington *et al.*<sup>6</sup> In this case, however, the spectra are much sparser and have not previously been assigned. We therefore use high-accuracy *ab initio* calculations to predict rovibronic levels, and then investigate feasible ways in which the potentials can be adjusted to give agreement with experiment. The adjustment is done using a variant of the “morphing” procedure of Meuwly and Hutson,<sup>7</sup> with energy and distance scaling factors for each of the spin-free potential curves. This procedure has antecedents in the work of Bowman and co-workers.<sup>8–11</sup>

Before considering HeN<sup>+</sup> in detail, it is useful to review the fine and hyperfine levels of the N<sup>+</sup> ion itself. The ground state of N<sup>+</sup> has a 2s<sup>2</sup>2p<sup>2</sup> configuration, which gives rise to <sup>1</sup>S, <sup>3</sup>P, and <sup>1</sup>D states. Only the <sup>3</sup>P state is important in the present discussion, with <sup>3</sup>P<sub>0</sub>, <sup>3</sup>P<sub>1</sub>, and <sup>3</sup>P<sub>2</sub> spin-orbit states. The <sup>3</sup>P<sub>1</sub> and <sup>3</sup>P<sub>2</sub> states lie 48.7385 cm<sup>-1</sup> and 130.7753 cm<sup>-1</sup>, respectively, above the <sup>3</sup>P<sub>0</sub> state. The <sup>14</sup>N nucleus has spin *I* = 1, so hyperfine structure can exist both through the nuclear magnetic moment and through the nuclear electric quadrupole moment. However, the quadrupole coupling is relatively weak, with a quadrupole constant *B* = -3.64 MHz.<sup>12,13</sup> The <sup>3</sup>P<sub>0</sub> state of the free N<sup>+</sup> ion has no hyperfine structure because of angular momentum constraints, and for the <sup>3</sup>P<sub>1</sub> state the magnetic coupling is so small that the quadrupole splitting dominates; the components of the <sup>3</sup>P<sub>1</sub> state are spread over only 13 MHz. For the <sup>3</sup>P<sub>2</sub> state the magnetic coupling is much larger (*A*<sub>2</sub> = 94.59 MHz) and the hyperfine levels are spread over 480 MHz.

If spin-orbit coupling is neglected, as in a standard *ab initio* calculation, He interacts with N<sup>+</sup> (<sup>3</sup>P) to produce two electronic states, <sup>3</sup>Σ<sup>-</sup> and <sup>3</sup>Π, with *Λ* = 0 and ±1, respec-

<sup>a)</sup>Electronic mail: Pavel.Soldan@durham.ac.uk

<sup>b)</sup>Electronic mail: J.M.Hutson@durham.ac.uk; Address for correspondence until 15 August 2002: J. M. Hutson, JILA, UCB 440, Boulder, Colorado 80309-0440.

tively. The  $\Sigma$  state corresponds to approach of He along the axis of the unoccupied  $p$  orbital, while the  $\Pi$  state corresponds to approach along the axis of one of the two singly-occupied  $p$  orbitals. Accordingly, the He atom can approach much closer for  $\Sigma$  than for  $\Pi$ , and the  $\Sigma$  curve is much deeper than the  $\Pi$  curve; the depths are approximately  $2000\text{ cm}^{-1}$  and  $200\text{ cm}^{-1}$ , respectively.

When spin-orbit coupling is included, the situation is considerably more complicated. At short range, where the spin-orbit coupling is small compared to the separation between the  $\Sigma$  and  $\Pi$  states,  $\Lambda$  is nearly conserved. At long range, however, where the spin-orbit coupling is large compared to the separation, the atomic total angular momentum  $J_a$  is nearly conserved. At both long and short range, the Born-Oppenheimer curves (though not necessarily the rovibronic levels) are characterized by a quantum number  $\Omega$ . At long range  $\Omega$  is the projection of  $J_a$  onto the internuclear axis and at short range it is  $\Lambda + \Sigma$ , the sum of the projections of the orbital and spin angular momenta. The resulting curves are qualitatively as shown in Fig. 1; it may be seen that the  $J_a=0$ ,  $\Omega=0$  and  $J_a=1$ ,  $|\Omega|=1$  curves correlate with the deep  ${}^3\Sigma$  well, while the remaining four curves correlate with the shallow  $\Pi$  well.

The projection  $\Omega$  is a good quantum number for the potential curves, but not for the rovibronic states. For  $J \neq 0$ , rotational (Coriolis) coupling connects states with  $\Delta\Omega = \pm 1$  and introduces  $\Omega$ -doubling, which splits a rovibronic state with  $|\Omega| \neq 0$  into parity-adapted combinations. Parity-adapted combinations with parity  $(-1)^J$  are called  $e$  levels, while those with parity  $(-1)^{J+1}$  are called  $f$  levels.<sup>14</sup> The  $e/f$  labeling is also used for  $\Omega=0$  levels, which are  $e$  states for  $J_a=0$  and  $2$  but are  $f$  states for  $J_a=1$ . Electric dipole transitions obey the selection rules  $\Delta J=0$ ,  $e \leftrightarrow f$  and  $\Delta J = \pm 1$ ,  $e \leftrightarrow e$  and  $f \leftrightarrow f$ .<sup>14</sup> (Vibronic states with  $\Omega=0, \pm 1$ , and  $\pm 2$  are also sometimes referred to as  $\Sigma$ ,  $\Pi$ , and  $\Delta$  states, respectively: this nomenclature should not be confused with that describing electronic states with  $\Lambda=0 \pm 1$ , etc., and is avoided in the present paper.)

## II. EXPERIMENTAL INFORMATION

The spectrum of  $\text{HeN}^+$  was first observed by Carrington *et al.*<sup>6</sup> using a mass-selected ion beam exposed to tunable microwave radiation. The experiment detects fragment ions produced either directly by the radiation or (more commonly) by electric field dissociation of high-lying bound states. It is thus sensitive only to transitions for which one level lies close to or above the dissociation limit.

Four structured transitions were observed in Ref. 6, at approximately 22.5, 31.5, 38.5, and 61.1 GHz. The 22.5, 31.5, and 38.5 GHz transitions showed resolved triplet hyperfine structure, while the 61.1 GHz transition appeared unsplit. Double resonance experiments performed later<sup>15</sup> showed that the 61.1 GHz single resonance is connected to both the 22.5 GHz triplet and 38.5 GHz transitions. The four energy levels involved must therefore lie near a single dissociation threshold. Moreover, the experiment showed that one energy level is involved in all three transitions. We will call this level the *central* level, and the remainder *end* levels. The hyperfine analysis also showed that the 61.1 GHz transition

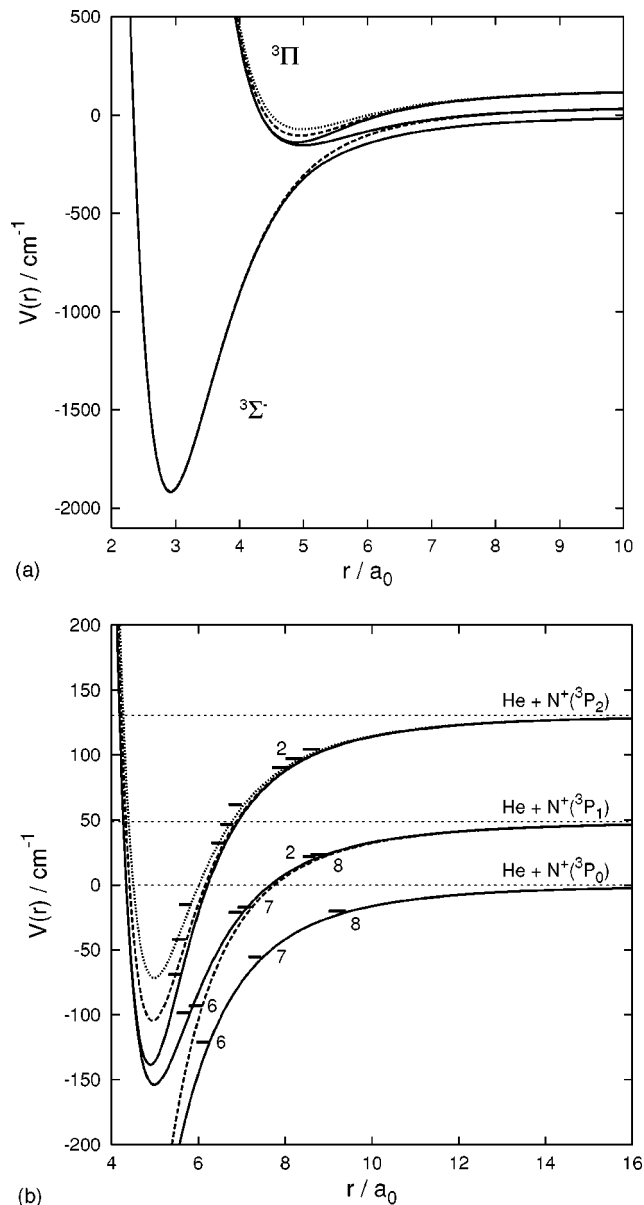


FIG. 1. Hund's case (c) potential energy curves for the  $\text{HeN}^+$  complex. (a) overview; (b) curves near dissociation. Solid curves correspond to  $\Omega=0$  states, dashed curves to  $|\Omega|=1$  states, and the dotted curve to the  $|\Omega|=2$  state. The labels against individual levels indicate vibrational quantum numbers.

is connected to all three components of the 22.5 and 38.5 GHz transitions. This means that the 61.1 GHz transition is in fact a triplet with very closely spaced hyperfine structure. The resulting energy level pattern is as shown in Fig. 2, with some possible variations: the whole level pattern can be turned upside-down, and the end level of the 61.1 GHz transition may be either above or below the central level; however, the end levels of the 22.5 and 38.5 GHz transitions must be on *opposite* sides of the central level.

There are several possible interpretations of the small hyperfine splitting of the 61.1 GHz transition. A pure Hund's case (c) state with  $\Omega=0$  has no magnetic hyperfine structure, even for  $J_a \neq 0$ . However, it must be remembered that neither  $J_a$  nor  $\Omega$  is accurately conserved in the complex, and it seems likely that Coriolis couplings (which mix states with

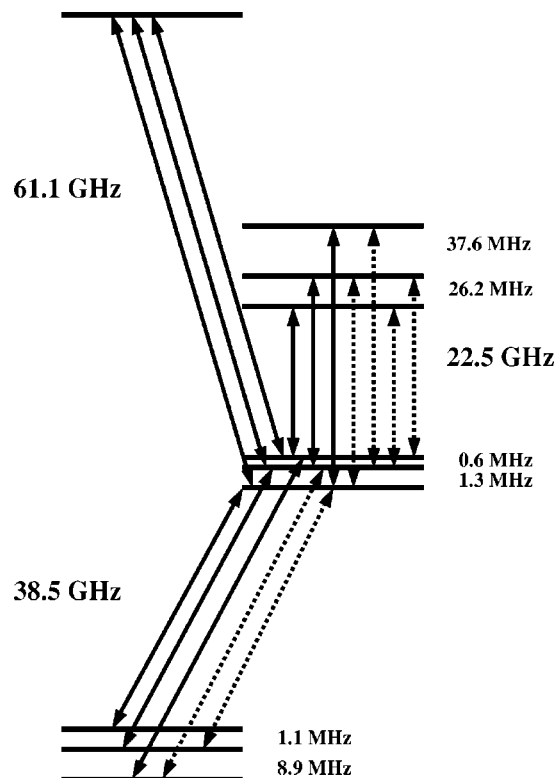


FIG. 2. The pattern of energy levels implied by the experimental data. Note that some variations are possible, as described in the text.

$\Delta\Omega = \pm 1$ ) will introduce significant hyperfine splittings for any level of the complex with  $J_a = 2$ , even if  $\Omega$  is nominally zero. Thus it seems likely that both levels involved in the 61.1 GHz transition have predominantly  $^3P_0$  or  $^3P_1$ ,  $\Omega = 0$  character. (This differs from the assignment suggested in Ref. 15, which is to a  $J_a = 2$  transition close to the  $^3P_2$  threshold.) Our assignment is supported by the absence of a measurable Zeeman effect for the 61.1 GHz transition; the Zeeman effect also vanishes for pure  $\Omega = 0$  states. The 22.5 and 31.5 GHz transitions broaden under an applied magnetic field, while the 38.5 GHz transition splits to give at least 19 partially resolved Zeeman components.<sup>15</sup> It was concluded from the Zeeman pattern that  $J$  for this transition is fairly low ( $J = 3$  or 4).

The double resonance experiments<sup>15</sup> revealed additional very weak hyperfine components and made it possible to assign the 22.5 GHz transition as  $\Delta J = 0$  and the 38.5 GHz transition as  $\Delta J = \pm 1$ .

The final piece of experimental information comes from the microwave power levels needed to observe the different transitions.<sup>6</sup> The 38.5 and 61.1 GHz transitions were observed at low power, and correspond to strong transitions. The 22.5 GHz and 31.5 GHz transitions required power levels a thousand times higher, so are much weaker. No other transitions were observed between 6 and 170 GHz despite extensive searching.

### III. THEORETICAL METHODS

#### A. Interaction potentials

The quality of an *ab initio* interaction potential depends greatly on the computational method and basis set employed.

Our aim is to generate potential energy curves at the highest affordable level of theory and then adjust them to fit experimental data. In the present work, we have used a spin-restricted open-shell variant<sup>16</sup> of the coupled-cluster method<sup>17</sup> with direct single and double excitations and a perturbative treatment of triples (RCCSD(T)). An augmented correlation-consistent polarized valence quintuple-zeta basis set<sup>18</sup> (aug-cc-pV5Z) was used (in its uncontracted form) for both He and N. In the He basis set we replaced 8 exponents of the  $1s$  orbital by 12 exponents. The resulting basis set contains 230 uncontracted Gaussian-type orbitals (GTOs), including higher angular momentum and diffuse basis functions. There are 86 GTOs on He ( $12s5p4d3f2g$ ) and 144 GTOs on N ( $15s9p5d4f3g2h$ ). All orbitals (not just valence orbitals) were correlated in the calculations.

The interaction potential  $\mathcal{V}(r)$  is defined as the electronic energy  $\mathcal{W}(r)$  of the complex with respect to that of the monomers. In practice, it is important to include the counterpoise (CP) correction for basis-set superposition error (BSSE),<sup>19</sup> so the monomer energies are also calculated in the complete supermolecular basis set and the interaction energy is calculated from

$$\mathcal{V}(r) = \mathcal{W}_{\text{HeN}^+}(r) - \mathcal{W}_{\text{He}}(r) - \mathcal{W}_{\text{N}^+}(r). \quad (1)$$

Comparison of the monomer energies with those calculated in the monomer basis set alone shows that the total BSSE is no larger than  $10 \text{ cm}^{-1}$  and  $2 \text{ cm}^{-1}$  in the regions of the  $^3\Sigma^-$  and  $^3\Pi$  potential wells, respectively. This indicates that BSSE is almost converged with respect to the basis set. [Note that RCCSD(T) calculations with the contracted aug-cc-pV5Z basis set give much larger counterpoise corrections, of  $62 \text{ cm}^{-1}$  and  $7 \text{ cm}^{-1}$ , respectively.] The CP-corrected interaction energies were calculated for 40 points on the  $^3\Sigma^-$  curve and 37 points on the  $^3\Pi$  curve, at bond lengths from  $1.6 a_0$  to  $30 a_0$ . The results are listed in Table I. All the *ab initio* calculations were carried out using the MOLPRO 2000.1 program suite.<sup>20</sup>

Potential energy curves  $V^\Sigma(r)$  and  $V^\Pi(r)$  were constructed from the *ab initio* points using the reciprocal power reproducing kernel Hilbert space interpolation procedure (RP-RKHS).<sup>21,22</sup> In order to obtain the correct long-range behavior of the interaction potential,

$$\mathcal{V}(r) \sim -\frac{C_4}{r^4} - \frac{C_6}{r^6} + \dots, \quad (2)$$

we interpolated with respect to  $r^2$  as described in Ref. 23 using the RP-RKHS parameters  $m = 1$  and  $n = 2$ . The resulting curves allow us to determine the corresponding equilibrium bond lengths  $r_e$  and the dissociation energies  $D_e$ . These are summarized in Table II and compared to previous *ab initio* calculations.<sup>24-26</sup> Using Eq. (9) of Ref. 23, we can also obtain the long-range coefficients of the interpolated curves. The  $C_4$  coefficients are  $0.6920 E_h a_0^4$  and  $0.6911 E_h a_0^4$  for  $^3\Sigma^-$  and  $^3\Pi$ , which compare well with the value  $0.6915 E_h a_0^4$ , based on the well-known dipole polarizability of He. The  $C_6$  coefficients are  $6.91 E_h a_0^6$  for  $^3\Sigma^-$  and  $2.84 E_h a_0^6$  for  $^3\Pi$ .

TABLE I. *Ab initio* interaction potentials from RCCSD(T) calculations with the aug-cc-pV5Z basis set for the  $^3\Sigma^-$  and  $^3\Pi$  states of  $\text{HeN}^+$ .

$r (a_0)$	$\mathcal{V}^\Sigma(r) (E_h)$	$\mathcal{V}^\Pi(r) (E_h)$	$r (a_0)$	$\mathcal{V}^\Sigma(r) (E_h)$	$\mathcal{V}^\Pi(r) (E_h)$
1.60	0.128 666 819	0.587 459 086	4.60	-0.002 579 312	-0.000 738 611
1.90	0.040 122 553	0.322 919 354	4.70	-0.002 347 131	-0.000 832 442
2.00	0.025 479 726	0.268 940 622	4.80	-0.002 136 991	-0.000 888 665
2.10	0.014 811 026	0.221 123 336	4.90	-0.001 947 040	-0.000 916 335
2.20	0.007 033 210	0.181 123 391	5.00	-0.001 775 496	-0.000 922 620
2.30	0.001 404 735	0.147 965 915	5.10	-0.001 620 664	-0.000 913 165
2.40	-0.002 600 761	0.120 561 108	5.20	-0.001 480 960	-0.000 892 385
2.50	-0.005 371 680	0.097 946 576	5.30	-0.001 354 911	-0.000 863 722
2.60	-0.007 204 022	0.079 310 934	5.40	-0.001 241 161	-0.000 829 811
2.70	-0.008 328 050	0.063 978 661	5.50	-0.001 138 470	-0.000 792 677
2.80	-0.008 924 438	0.051 388 641	5.70	-0.000 961 867	-0.000 714 447
2.90	-0.009 134 801	0.041 074 249	6.00	-0.000 755 049	-0.000 600 095
3.00	-0.009 069 332	0.032 646 642	6.50	-0.000 519 036	-0.000 440 775
3.10	-0.008 812 818	0.025 781 313	7.00	-0.000 368 966	-0.000 324 739
3.20	-0.008 429 631	0.020 207 240	8.00	-0.000 202 725	-0.000 184 846
3.30	-0.007 967 930	0.015 698 084	10.00	-0.000 077 388	-0.000 072 842
3.70	-0.005 911 285	0.004 977 173	15.00	-0.000 014 328	-0.000 013 929
4.00	-0.004 533 783	0.001 490 051	20.00	-0.000 004 437	-0.000 004 366
4.20	-0.003 765 221	0.000 286 976	30.00	-0.000 000 864	-0.000 000 857
4.50	-0.002 835 415	-0.000 595 799	50.00	-0.000 000 112	-0.000 000 111

As mentioned above, the splitting between the spin-free  $^3\Sigma^-$  and  $^3\Pi$  states in the long-range region ( $R > 6 a_0$ ) is comparable to or smaller than the spin-orbit coupling. Under these circumstances, the projection quantum numbers  $\Lambda$  and  $\Sigma$  [Hund's case (a)] do not provide an adequate characterization of the curves near dissociation. Instead, the curves are labeled by quantum numbers  $J_a$  and  $|\Omega|$  for the total angular momentum of the  $\text{N}^+$  atomic ion and its projection onto the interatomic axis. The  $^3P_0$  ground state of  $\text{N}^+$  gives rise to an  $\Omega = 0$  state, the  $^3P_1$  state gives rise to  $|\Omega| = 0$  and 1, and  $^3P_2$  gives rise to  $|\Omega| = 0, 1$ , and 2.

The case (c) potential energy curves of  $\text{HeN}^+$  were obtained from the spin-free  $^3\Sigma^-$  and  $^3\Pi$  curves by assuming that the atomic  $L$  and  $S$  quantum numbers are conserved in the molecular ion and that the spin-orbit operator retains its atomic form [diagonal in the case (c) basis set] at all interatomic distances. Experimental values<sup>12,13</sup> of 48.7385 and 82.0368  $\text{cm}^{-1}$  were used for the energy separations between the  $^3P_0$ ,  $^3P_1$ , and  $^3P_2$  spin-orbit states of  $\text{N}^+$ . The resulting

curves are shown in Fig. 1. The corresponding equilibrium bond lengths  $r_e$  and dissociation energies  $D_e$  are listed in Table III. The curves are significantly deeper than the *ab initio* MRD-CI curves by Buenker and Gu,<sup>27</sup> where the spin-orbit coupling was taken into account *a priori*. This difference may be attributed mostly to the significantly larger basis set used to generate the spin-free curves in the present study, rather than to the approximations introduced in the spin-orbit treatment here or to the different *ab initio* method used by Buenker and Gu.<sup>27</sup> To verify this, we carried out single-point MRCI calculations at the potential minima, using the same basis set as for the RCCSD(T) calculations. The resulting well depths were 1981  $\text{cm}^{-1}$  and 200  $\text{cm}^{-1}$  for the  $^3\Sigma^-$  and  $^3\Pi$  states, respectively. These cannot be corrected for BSSE at the MRCI level, because the MRCI method is not size-consistent. However, assuming that the BSSE correction is the same for MRCI as for RCCSD(T), this suggests well depths of 1971  $\text{cm}^{-1}$  and 198  $\text{cm}^{-1}$ , respectively.

TABLE II. *Ab initio* values of  $D_e$  ( $\text{cm}^{-1}$ ) and  $r_e$  ( $a_0$ ) for spin-free curves of  $\text{HeN}^+$  [in a Hund's case (a) representation].

Authors	$^3\Sigma^-$		$^3\Pi$	
	$D_e$ ( $\text{cm}^{-1}$ )	$r_e$ ( $a_0$ )	$D_e$ ( $\text{cm}^{-1}$ )	$r_e$ ( $a_0$ )
Cooper and Wilson <sup>a</sup>	600	3.83	...	...
Frenking <i>et al.</i> <sup>b</sup>	1435	3.305	...	...
Gu <i>et al.</i> <sup>c</sup>	1414	3.083	31	5.444
This work <sup>d</sup>	2006	2.922	202	4.985
This work <sup>e</sup>	1954	2.922	192	4.985
This work <sup>f</sup>	1961	2.922	192	4.985

<sup>a</sup>SCF; Ref. 24.

<sup>b</sup>MP2; Ref. 25.

<sup>c</sup>MRD-CI; Ref. 26.

<sup>d</sup>RCCSD(T); see text.

<sup>e</sup>Scaled potential SH1; see text.

<sup>f</sup>Scaled potential SH0; see text.

## B. Bound and quasibound states

The methods used to carry out bound-state calculations on  $\text{HeN}^+$  in the present work are almost exactly the same as those described in Ref. 3. The Schrödinger equation for each total angular momentum  $J$  and total parity is written as a set of coupled differential equations in a Hund's case (e) basis set.<sup>28</sup> The basis functions are described by quantum numbers  $L$ ,  $S$ , and  $J_a$  for the atomic ion, the end-over-end (mechanical rotation) quantum number  $R$ , and the total angular momentum  $J$ . The case (e) basis functions do not have any quantum numbers describing projections of angular momenta onto the internuclear axis. The interaction potential, the rotational coupling and the atomic spin-orbit coupling are all fully taken into account. The atomic  $L$  and  $S$  quantum numbers are taken to be conserved in the molecular ion; the spin-orbit operator is assumed to retain its atomic form at all inter-

TABLE III. Values of  $D_e$  (cm<sup>-1</sup>) and  $r_e$  (a<sub>0</sub>) (in parentheses) of HeN<sup>+</sup> in Hund's case (c) representation.

$J_a$	0		1		2	
	0	0	1	0	1	2
Buenker and Gu <sup>a</sup>	1596 (3.0)	157 (5.1)	1646 (3.0)	226 (4.9)	193 (5.0)	157 (5.1)
This work <sup>b</sup>	1919 (2.92)	203 (4.99)	1965 (2.92)	269 (4.90)	235 (4.95)	203 (4.99)
This work <sup>c</sup>	1868 (2.92)	192 (4.99)	1914 (2.92)	259 (4.90)	225 (4.95)	192 (4.99)
This work <sup>d</sup>	1875 (2.92)	193 (4.99)	1921 (2.92)	260 (4.90)	225 (4.95)	193 (4.99)

<sup>a</sup>MRD-CI; Ref. 27.<sup>b</sup>Derived from unmorphed spin-free potential energy curves; see text.<sup>c</sup>Scaled potential SH1; see text.<sup>d</sup>Scaled potential SH0; see text.

atomic distances, and experimental values are used for the energies of the free atomic ion (threshold energies).

The parity of the basis functions is important in understanding the allowed transitions and dissociation processes. All the states of N<sup>+</sup> arising from a  $2p^2$  configuration have even parity, regardless of  $J_a$ , so that the parity of the case (e) functions is simply  $(-1)^R$ . The lowest dissociation channel for  $e$  levels [parity  $(-1)^J$ ] correlates with the N<sup>+</sup>(<sup>3</sup>P<sub>0</sub>) dissociation limit, while for  $f$  levels [parity  $(-1)^{J+1}$ ] it correlates with the He+N<sup>+</sup>(<sup>3</sup>P<sub>1</sub>) limit. Therefore, in the energy region between the <sup>3</sup>P<sub>0</sub> and <sup>3</sup>P<sub>1</sub> thresholds, the  $f$  levels are bound and the  $e$  levels can predissociate.

The bound-state calculations in the present work were carried out using the BOUND program.<sup>29,30</sup> The coupled equations were solved subject to bound-state boundary conditions using the diabatic modified log-derivative method,<sup>31</sup> with a grid from 0.9 Å to 27.0 Å. The equations were solved using step sizes  $h=0.005$  Å and 0.01 Å and the results were extrapolated to zero step size using Richardson  $h^4$  extrapolation.<sup>29</sup> The resulting eigenvalues are converged to better than 1 MHz.

Positions and widths of quasibound states were determined by the method of Ashton, Child, and Hutson.<sup>32</sup> The  $S$  matrix eigenphase sum spectrum was obtained by close-coupled scattering calculations at many energies across each resonance, using the MOLSCAT program.<sup>33</sup> The coupled equations were again solved using the diabatic modified log-derivative method,<sup>31</sup> for step size 0.01 Å and a grid from 0.9 Å to 67.0 Å. The eigenphase sums near the resonance were then fitted to the generalized Breit–Wigner formula<sup>34</sup> to give the position and width of the quasibound state. The fitting was performed using the RESFIT program.<sup>35</sup>

The results of the calculations are given in Tables IV, V, and VI. The coupled-channel calculations give numerically exact energy levels, including all nonadiabatic couplings within the manifold of electronic states included. However, they do not give quantum number assignments directly. To obtain such assignments, we also solved the Schrödinger equation using the LEVEL program<sup>36</sup> for each adiabatic potential energy curve. The curves were obtained by diagonalizing the electronic and spin–orbit Hamiltonian for each value of  $|\Omega|$  on a grid on internuclear distances, including the diagonal centrifugal term (but not the Coriolis terms off-diagonal in  $\Omega$ ). The resulting energy levels are included in Tables IV, V, and VI and shown in Fig. 1(b). The adiabatic energy level pattern is close enough to the one from the

coupled-channel calculations to allow unambiguous assignment of case (c) quantum numbers to nearly all the levels. The  $|\Omega|$  labels are approximate, because they neglect derivative couplings and the rotational (Coriolis) coupling between levels that differ by  $\Delta\Omega = \pm 1$ , but they are nevertheless conceptually useful. The  $J_a$  labels are more approximate still, because even at the adiabatic level the electronic Hamiltonian mixes levels with different  $J_a$  for a given  $\Omega$ .

### C. Potential and coordinate scaling

*Ab initio* potentials, even if calculated at a very high level of theory, are not usually accurate enough to reproduce spectroscopic results exactly. However, such potentials provide a good starting point for potential scaling or morphing<sup>7</sup> to achieve agreement with the experimental data. In this pa-

TABLE IV. Calculated Hund's case (c) levels ( $E_c$ ) and the corresponding coupled-channel levels and their widths ( $E$  and  $\Gamma$ ) for  $\Omega=0$  curves and  $J=0$  on the unmorphed RCCSD(T) potential. The two coupled-channel levels marked with \* are strongly mixed combinations of  $J_a=0$  and 2.

$J_a$	$\nu$	$E_c$ (cm <sup>-1</sup> )	$E$ (cm <sup>-1</sup> )	$\Gamma$ (cm <sup>-1</sup> )	$e/f$	
0	0	-1686.12	-1686.1179	...	$e$	
	1	-1280.06	-1280.0431	...	$e$	
	2	-931.11	-931.0630	...	$e$	
	3	-638.98	-638.8086	...	$e$	
	4	-404.52	-403.8883	...	$e$	
	5	-231.41	-230.6338	...	$e$	
	6	-120.87	-126.8791	...	$e$	
	7	-55.18	-53.6686*	...	$e$	
	8	-20.38	-22.5255	...	$e$	
	9	-5.42	-6.3035	...	$e$	
	10	-0.75	-0.9603	...	$e$	
1	0	-98.56	-98.5611	...	$f$	
	1	-21.28	-21.2790	...	$f$	
	2	21.66	21.6627	...	$f$	
	3	40.98	40.9840	...	$f$	
	4	47.51	47.5090	...	$f$	
	5	48.71	48.7217	...	$f$	
	2	0	-69.03	-63.5949*	...	$e$
		1	32.22	40.0803	1.3795	$e$
		2	90.37	94.3738	0.4901	$e$
		3	118.10	119.7363	0.1608	$e$
		4	128.41	128.8824	0.0414	$e$
5	130.72	130.7754	0.0024	$e$		

TABLE V. Calculated Hund's case (c) levels ( $E_c$ ) and the corresponding  $e/f$  coupled-channel levels ( $E$ ) and their widths ( $\Gamma$ ) for  $|\Omega|=1$  curves and  $J=1$  on the unmorphed RCCSD(T) potential. Coupled channel levels indicated with \* cannot be assigned unambiguously in terms of case (c) quantum numbers.

$J_a$	$v$	$E_c$ (cm $^{-1}$ )	$e$ state		$f$ state	
			$E$ (cm $^{-1}$ )	$\Gamma$ (cm $^{-1}$ )	$E$ (cm $^{-1}$ )	$\Gamma$ (cm $^{-1}$ )
1	0	-1683.25	-1676.3595	...	-1683.2467	...
	1	-1276.99	-1270.9096	...	-1276.9915	...
	2	-927.67	-922.5161	...	-927.6581	...
	3	-634.67	-630.6661	...	-634.6119	...
	4	-397.74	-395.2769	...	-397.5433	...
	5	-217.17	-216.3129	...	-216.8196	...
	6	-92.86	-95.3146	...	-94.8762	...
	7	-17.25	-19.1338	...	-18.4985	...
	8	23.54	22.4630	0.0279	23.3336	...
	9	41.69	41.2837	0.1855	41.9208*	...
	10	47.69	47.5724	0.0118	47.8996*	...
2	0	-41.84	-38.0662	...	-37.0623	...
	1	46.73	50.1015	0.2452	49.3940	0.1359
	2	97.40	99.5322	0.1808	98.6916	0.1094
	3	120.93	122.1920*	0.0872	121.4280	0.0548
	4	129.21	129.8162*	0.0243	129.3377	0.0157

per we investigate both potential and coordinate scaling to modify the *ab initio* potential energy curves. The resulting curves are represented as

$$V_{\text{scaled}}^X(\eta_X, \rho_X; r) = \eta_X V^X(\rho_X r), \quad (3)$$

where  $X = \Sigma$  or  $\Pi$ . The scaling parameters  $\eta_X$ ,  $\rho_X$ ,  $\eta_{\Pi}$ , and  $\rho_{\Pi}$  are determined by least-squares fits to the experimental transition frequencies making use of the I-NOLLS program.<sup>37</sup>

#### IV. RESULTS AND DISCUSSION

We have calculated all the bound and quasibound rovibronic states of  $\text{HeN}^+$  for  $J \leq 5$  on the unmorphed RCCSD(T) potential. Above  $J=5$  the levels are very sparse, and groups of levels that could produce the double-resonance results do not exist. The levels immediately below each of the three dissociation limits are shown in Figs. 3, 4, and 5. The levels below the  $^3P_0$  threshold (Fig. 3) show a pattern typical of Hund's case (c); each level has a reasonably well-defined  $\Omega$  quantum number, with the levels forming identifiable rotational progressions starting at  $J=|\Omega|$ . Close to the  $^3P_1$  threshold, however, the level pattern is quite different (Fig. 4). The progression starting around 41.5 cm $^{-1}$  can be satisfactorily explained in terms of case (c) quantum numbers, but the pattern of the higher levels is characteristic of

Hund's case (e): there are no pairings of odd and even parity levels for a given value of  $|\Omega|$ , but instead the levels are grouped into "horizontal" sets of three, of the same parity and thus alternating  $e/f$  character, corresponding to states with the same value of the rotational quantum number  $R$  and  $J=R-1$ ,  $R$  and  $R+1$ . This arises in much the same way as in  $\text{HeKr}^+$  (Ref. 4): there is a close near-degeneracy between the vibrational levels  $J_a=1$ ,  $\Omega=0$ ,  $v=4$  and  $J_a=1$ ,  $|\Omega|=1$ ,  $v=10$ , and to a lesser extent between the corresponding  $\Omega=0$ ,  $v=3$  and  $|\Omega|=1$ ,  $v=9$  levels; the near-degenerate  $\Omega=0$  and 1 levels are then completely mixed by the rotational (Coriolis) coupling. Below the  $^3P_2$  threshold (Fig. 5), the pattern is a complicated one that is not close to either case (c) or case (e).

One feature of the energy level diagrams is at first sight surprising, at least to those familiar with the energy levels of atom-diatom van der Waals complexes, which are in many ways closely analogous. This is that  $J_a=1$  levels with  $J=0$  (and thus  $\Omega=0$ ) have odd rather than even parity and are thus  $f$  levels. For atom-diatom van der Waals complexes, all  $J=0$  levels have even parity. The difference arises because the  $^3P_1$  state of  $\text{N}^+$  itself has even parity, by contrast to the  $j=1$  state of a diatomic molecule which has odd parity.

TABLE VI. Calculated Hund's case (c) levels ( $E_c$ ) and the corresponding  $e/f$  coupled-channel levels ( $E$ ) and their widths ( $\Gamma$ ) for  $|\Omega|=2$  curve and  $J=2$  on the unmorphed RCCSD(T) potential. Coupled channel levels indicated with \* cannot be assigned unambiguously in terms of case (c) quantum numbers.

$J_a$	$v$	$E_c$ (cm $^{-1}$ )	$e$ state		$f$ state	
			$E$ (cm $^{-1}$ )	$\Gamma$ (cm $^{-1}$ )	$E$ (cm $^{-1}$ )	$\Gamma$ (cm $^{-1}$ )
2	0	-15.11	-14.7659	...	-14.7134	...
	1	61.87	62.3140	0.0144	62.2737	0.0099
	2	104.48	105.1233	0.0346	104.9641	0.0138
	3	123.49	124.5302*	0.0607	124.0111*	0.0140
	4	129.75	130.6361*	0.0128	130.1656*	0.0063

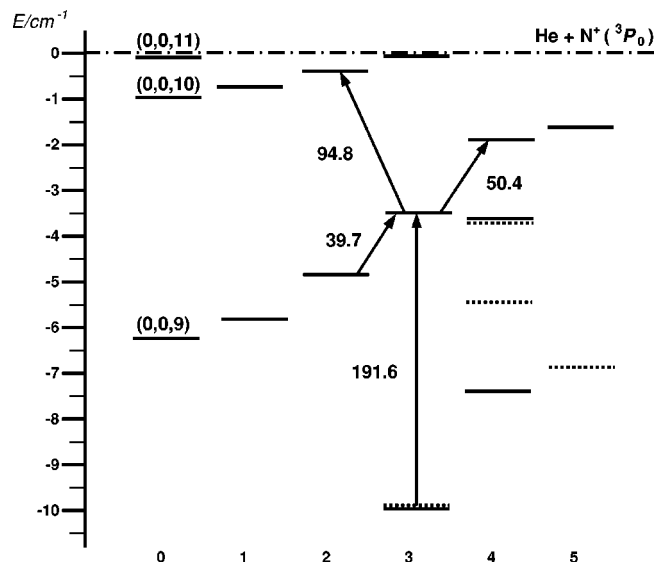


FIG. 3. Energy level diagram below the He+N<sup>+</sup>(<sup>3</sup>P<sub>0</sub>) dissociation limit. The energy levels are arranged in columns according to the values of  $J$ . The  $f$  levels are shown by dashed lines and  $e$  levels by continuous lines. All energy levels correspond to bound states. Solid arrows represent transitions used in subsequent scaling. The transition frequencies are in GHz. The origins of rotational sequences are labeled by  $(J_a, |\Omega|, \nu)$ .

The first experimental question to be addressed is which of the thresholds is involved in the group of transitions connected by double resonance. We need to find four levels in the right pattern, connected by transitions at approximately 61.1, 38.5, and 22.5 GHz. The calculated levels are clearly densest near the <sup>3</sup>P<sub>2</sub> and <sup>3</sup>P<sub>1</sub> thresholds, so at first sight these seem to offer attractive possibilities. However, on closer inspection it turns out that the widths of the quasibound states are not compatible with such an assignment. The transitions involved in double resonance are all sharp, with line widths around 1 MHz ( $3 \times 10^{-5}$  cm<sup>-1</sup>). Between the <sup>3</sup>P<sub>1</sub> and <sup>3</sup>P<sub>2</sub> thresholds, *all* the levels are quasibound,

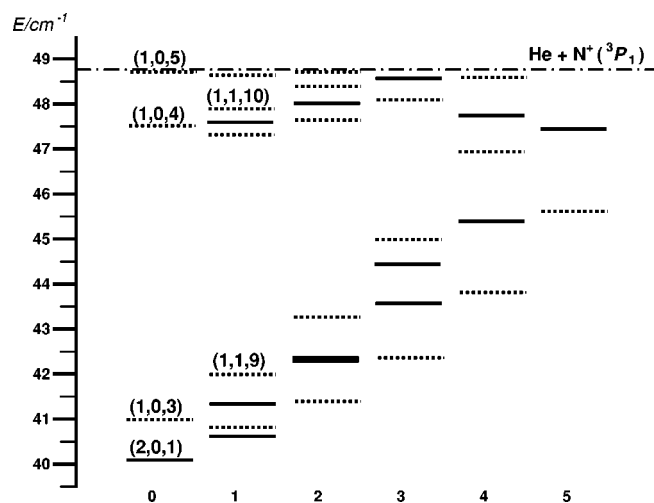


FIG. 4. Energy level diagram below the He+N<sup>+</sup>(<sup>3</sup>P<sub>1</sub>) dissociation limit. The energy levels are arranged in columns according to the values of  $J$ . The  $f$  levels, shown by dashed lines, correspond to bound states. The  $e$  levels, shown by continuous lines, correspond to quasibound states. The origins of rotational sequences are labeled by  $(J_a, |\Omega|, \nu)$ .

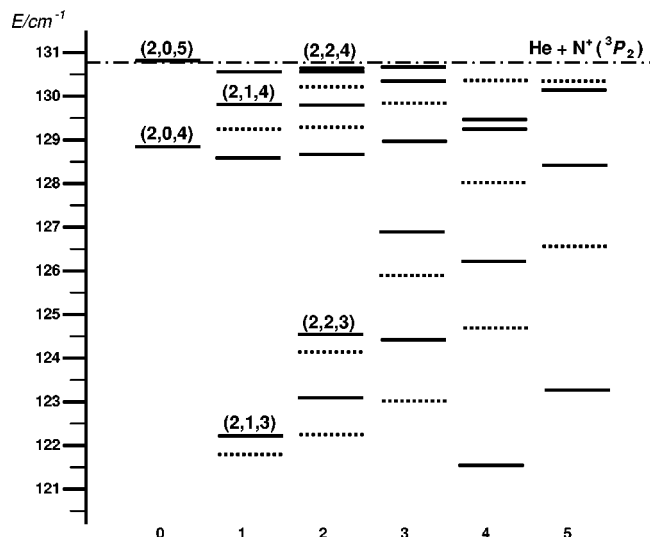


FIG. 5. Energy level diagram below the He+N<sup>+</sup>(<sup>3</sup>P<sub>2</sub>) dissociation limit. The energy levels are arranged in columns according to the values of  $J$ . The  $f$  levels are shown by dashed lines and  $e$  levels by continuous lines. All energy levels correspond to quasibound states. The origins of rotational sequences are labeled by  $(J_a, |\Omega|, \nu)$ .

with calculated widths ranging from  $9.7 \times 10^{-4}$  cm<sup>-1</sup> to 1.36 cm<sup>-1</sup>. Between the <sup>3</sup>P<sub>0</sub> and <sup>3</sup>P<sub>1</sub> thresholds,  $e$  levels [parity  $(-1)^J$ ] are quasibound while  $f$  levels [parity  $(-1)^{J+1}$ ] are bound. The  $\Delta J = \pm 1$  transitions could thus be bound-bound transitions, but as discussed above the 22.5 GHz transition is assigned as  $\Delta J = 0$ , so would have to involve a quasibound level if it was above the <sup>3</sup>P<sub>0</sub> threshold. The narrowest quasibound states that we have identified in this region are  $e$  levels that in a case (c) description belong to sequences with  $J_a = 1$ ,  $|\Omega| = 1$  for  $\nu = 8, 9$ , and 10. In a case (e) description, they have  $R = J$ . The widths range from 0.012 cm<sup>-1</sup> ( $J = 1$ ,  $\nu = 10$ ) to 0.442 cm<sup>-1</sup> ( $J = 5$ ,  $\nu = 8$ ). Even the narrowest of these are not consistent with the sharp lines observed experimentally.

Levels arising from  $J_a = 2$ ,  $|\Omega| = 1$  or 2 might also produce narrow quasibound states. However, there are no  $|\Omega| = 2$  levels that could be shifted to near the <sup>3</sup>P<sub>1</sub> threshold by a plausible change in the potential, and the  $J_a = 2$ ,  $|\Omega| = 1$   $e$  states are found to be far too broad to give sharp lines in the spectrum.

We thus conclude that the four states involved in the transitions connected by double resonance all lie just below the <sup>3</sup>P<sub>0</sub> threshold.

Before looking for a more specific assignment, it is important to understand how sensitive the different levels are to small changes in the potential curves, especially the well depths. It is reasonable to suppose that the RCCSD(T) curves could have well depths that are in error by up to about 3% for <sup>3</sup>Σ and up to about 10% for <sup>3</sup>Π (because of the larger contribution of dispersion in the latter case). This corresponds to about 15% of a vibrational spacing (near the minimum) for the Σ curve and about 20% of a vibrational spacing for the Π curve. For near-dissociation levels that lie on the dissociating curve, the vibrational spacing near dissociation is low, so the level positions are relatively insensitive to

such changes in the potential: the levels slide up or down the curve a little as the depth changes, and the rotational spacings (for a given  $J, J'$ ) decrease or increase slightly as the levels slide up or down. However, the effects are not drastic. For levels that belong to *higher* curves, by contrast, the local vibrational spacing is still large near the  ${}^3P_0$  threshold, so much larger changes in energy can be caused by small changes in the potential.

The  $\Delta J=0$  transition at 22.5 GHz has a large hyperfine splitting, so must involve a state with  $J_a > 0$  character. Its frequency is thus likely to be very strongly potential-dependent, so we defer attempting to assign it. However, the 38.5 and 61.1 GHz transitions, with  $\Delta J = \pm 1$ , plausibly involve levels that lie on the curve that is dissociating to  $N^+$  ( ${}^3P_0$ ), whose energies should be relatively weakly potential-dependent. The 38.5 GHz transition is very strong, and is at too low a frequency to be a vibrational transition; by far the best candidate for it is the  $J=3 \leftarrow 2$  transition for  $v=9$  of the curve correlating with  $N^+$  ( ${}^3P_0$ ), which lies at 39.7 GHz on the unmorphed potential. This can be brought into agreement with experiment by making the  $\Sigma$  potential slightly shallower (by about 2%), so that the levels move up towards dissociation and to correspondingly larger distance.

The assignment of the 61.1 GHz transition is less clear-cut. It could be the  $J=4 \leftarrow 3$  transition in the same sequence as the 38.5 GHz transition. However, if the potential is morphed to reduce the frequency of the  $J=3 \leftarrow 2$  transition from 39.7 to 38.5 GHz, that of the  $J=4 \leftarrow 3$  transition will also be reduced, from 50.4 GHz, unless a specific level interaction (perturbation) shifts one of the levels. Such a perturbation is not implausible, but there is another possibility: moving the  $v=9$  level up the well to reduce its rotational constant could bring the  $v=10 \leftarrow 9$ ,  $J=2 \leftarrow 3$  transition down from 94.8 GHz to the required 61.1 GHz.

If the 38.5 GHz transition is a pure rotational  $J=3 \leftarrow 2$  transition, the fact that there is much more hyperfine splitting in one of its levels than the other requires explanation. This issue will be addressed below.

There is no good frequency match on the unmorphed potential for the 22.5 GHz transition. As discussed above, this transition is assigned experimentally as  $\Delta J=0$ , and the large hyperfine splitting of its end level suggests the assignment  $J_a=2$ . It may be seen that there is indeed a  $J_a=2$ ,  $|\Omega|=2$   $f$  level, 191.1 GHz below the central level on the unmorphed potential. As discussed above, levels correlating with higher thresholds are expected to be very sensitive to energy scaling, and test calculations confirm that this level is very sensitive to the scaling of the  ${}^3\Pi$  curve. It may be brought up to the required 22.5 GHz above the central level by reducing the depth of the  $\Pi$  potential by about 5%.

We thus have two possible assignments of the three transitions connected by double resonance, which differ only in the assignment of the 61.1 GHz transition as  $\Delta v=0$  or  $\Delta v=1$ . We have carried out least-squares fits to optimize potential scaling parameters for both these assignments. We investigated both two-parameter fits (with energy scaling factors  $\eta_\Sigma$  and  $\eta_\Pi$ ) and three-parameter fits (with an additional single distance scaling factor  $\rho_\Sigma = \rho_\Pi$ ). Since we are fitting to only three experimental frequencies, the three-parameter

TABLE VII. Scaling parameters for the fitted SH0 and SH1 potentials. Statistical 95% confidence limits in the last digits are given in parentheses.

Potential	$\eta_\Sigma$	$\rho_\Sigma$	$\eta_\Pi$	$\rho_\Pi$
SH0	0.977 75 (699)	1.0	0.950 66 (322)	1.0
SH1	0.974 20 (871)	1.0	0.949 90 (265)	1.0

fits are capable of giving an essentially exact fit to the data. However, the  $\eta_\Sigma$  parameters in the three-parameter fits are uncomfortably small ( $<0.97$ ), so we list here only the two-parameter fits; the fitted parameters are given in Table VII. The two potentials arising from the  $\Delta v=0$  and 1 assignments will be referred to as the SH0 and SH1 potentials respectively. The corresponding calculated level patterns near the  $N^+$   ${}^3P_0$  threshold are shown in Figs. 6 and 7.

We cannot choose conclusively between the  $\Delta v=0$  and  $\Delta v=1$  assignments at this point. However, the hyperfine splittings of the 38.5 GHz and 61.1 GHz lines suggest that the  $\Delta v=1$  assignment is preferable. The theory of the hyperfine splittings is complicated, because of the presence of both magnetic and quadrupole couplings, and is beyond the scope of the present paper. It will be developed in detail in a future publication. However, our preliminary calculations indicate that the  $J=2$  and  $J=4$  levels of the  $\Omega=0$ ,  $v=9$  progression both have significant magnetic hyperfine splittings, because of mixing in of  $J_a=2$  character. The  $J=3$  level also has a significant hyperfine splitting on the unmorphed potential, but on the morphed potentials its hyperfine splitting is very small because of an accidental cancellation of contributions. This satisfactorily explains the very small hyperfine splittings observed for the central level. Nevertheless, for the  $\Delta v=1$  assignment, the 61.1 GHz line would be expected to show hyperfine structure because of the splitting of the  $v=9$ ,  $J=4$  level. The  $v=10$ ,  $J=2$  level, by contrast, has a

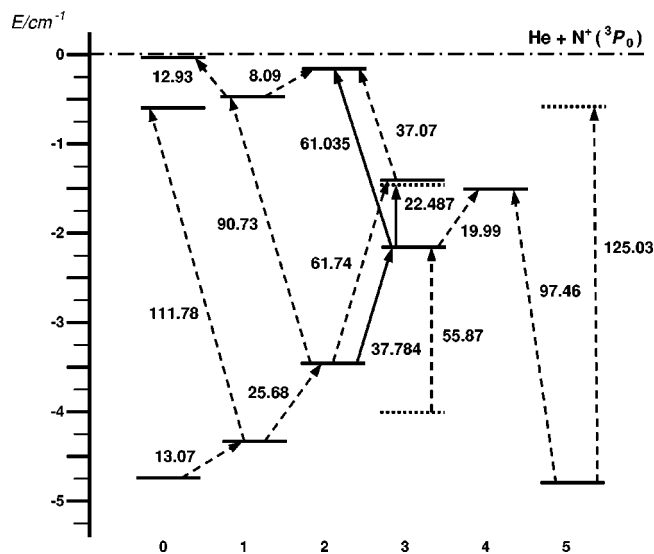


FIG. 6. Energy level diagram below the  $He+N^+$  ( ${}^3P_0$ ) dissociation limit for morphed potential SH1. The energy levels are arranged in columns according to the values of  $J$ . The  $f$  levels are shown by dashed lines and  $e$  levels by continuous lines. All energy levels correspond to bound states. Solid arrows represent fitted transitions and dashed arrows represent predicted transitions. The transition frequencies are in GHz.

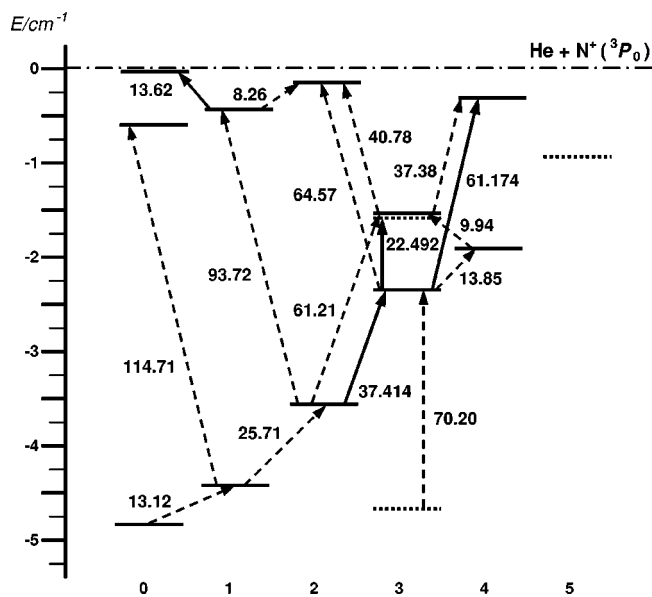


FIG. 7. Energy level diagram below He+N<sup>+</sup>(<sup>3</sup>P<sub>0</sub>) dissociation limit for the morphed potential SH0. The energy levels are arranged in columns according to the values of *J*. The *f* levels are shown by dashed lines and *e* levels by continuous lines. All energy levels correspond to bound states. Solid arrows represent fitted transitions and dashed arrows represent predicted transitions. The transition frequencies are in GHz.

very small hyperfine splitting, because it is an almost pure <sup>3</sup>P<sub>0</sub> state. The lack of an observable hyperfine splitting in the 61.1 GHz transition thus favors the Δ*v*=1 assignment.

A complete set of calculated transition frequencies and intensities between levels within 5 cm<sup>-1</sup> of dissociation is given in Tables VIII and IX for the SH1 and SH0 potentials respectively. The intensities neglect population factors, and are calculated simply as squares of dipole moment matrix

elements, assuming that the dipole moment operator is simply  $erm_{\text{He}}/(m_{\text{He}}+m_{\text{N}})$ , corresponding to a charge of +*e* on the N atom. Observation of further transitions would provide the most satisfactory confirmation of our assignment. It should be remembered that only transitions that end on levels within about 4 cm<sup>-1</sup> of dissociation are likely to be observed in single-resonance experiments, because of the need for electric field dissociation. In addition, it has been found for HeAr<sup>+</sup> (Ref. 3) and HeKr<sup>+</sup> (Ref. 4) that transitions originating in levels in the top 0.5 cm<sup>-1</sup> of the well tend not to be observed, presumably because such levels are not strongly populated in the ion source.

The calculated intensities provide further evidence for the Δ*v*=1 assignment; for the SH0 potential, the *v*=10 ← 9, *J*=2 ← 3 transition at 64.58 GHz is only a factor of 7 weaker than the *v*=9, *J*=4 ← 3 transition, and would probably have been seen experimentally. By contrast, for the SH1 potential, the *v*=9, *J*=4 level has been pushed up out of the well; the lack of an observed transition to it is thus no obstacle to the Δ*v*=1 assignment.

We are not aware of any previous calculation of the energies and widths of quasibound states in a system such as this. Accordingly, we list in Tables X and XI the energies and widths of states lying just below the <sup>3</sup>P<sub>1</sub> and <sup>3</sup>P<sub>2</sub> thresholds, calculated on the SH1 potential. Once again, it may be seen that the narrowest quasibound states below the <sup>3</sup>P<sub>1</sub> threshold are the *e* states with *J*<sub>*a*</sub>=1, which have |Ω|=1 in a case (c) description and *R*=*J* in a case (e) description. These states are narrow because the predissociation is a third-order process: the potential does not couple *J*<sub>*a*</sub>=1 to *J*<sub>*a*</sub>=0 and 2 for Ω=0, so the only route is

$$(J_a, |\Omega|) = (1, 1) \xleftrightarrow{\text{potential}} (2, 1) \xleftrightarrow{\text{Coriolis}} (2, 0) \xleftrightarrow{\text{potential}} (0, 0). \quad (4)$$

TABLE VIII. Calculated transition frequencies (in GHz) for the morphed SH1 potential.

Upper state					Lower state					Frequency (GHz)	
<i>J</i> <sub><i>a</i></sub>	Ω	<i>v</i>	<i>J</i>	<i>e/f</i>	<i>J</i> <sub><i>a</i></sub>	Ω	<i>v</i>	<i>J</i>	<i>e/f</i>	Calc. (Int.)	Obs.
2	2	0	3	<i>e</i>	2	2	0	3	<i>f</i>	1.4734 (2.3-01)	...
2	2	0	3	<i>e</i>	1	1	7	4	<i>e</i>	3.9713 (1.4-03)	...
0	0	10	1	<i>e</i>	0	0	10	0	<i>e</i>	4.6270 (4.1+00)	...
0	0	10	2	<i>e</i>	0	0	10	1	<i>e</i>	8.0888 (1.1+00)	...
0	0	11	0	<i>e</i>	0	0	10	1	<i>e</i>	12.9327 (8.6-02)	...
0	0	9	1	<i>e</i>	0	0	9	0	<i>e</i>	13.0733 (1.4+00)	...
1	1	7	4	<i>e</i>	0	0	9	3	<i>e</i>	19.9895 (7.5-02)	...
2	2	0	3	<i>f</i>	0	0	9	3	<i>e</i>	22.4875 (4.7-03)	22.4842
0	0	9	2	<i>e</i>	0	0	9	1	<i>e</i>	25.6759 (3.5-01)	...
0	0	10	2	<i>e</i>	2	2	0	3	<i>e</i>	37.0741 (9.2-04)	...
0	0	9	3	<i>e</i>	0	0	9	2	<i>e</i>	37.7841 (1.9-01)	38.5031
0	0	9	3	<i>e</i>	1	1	7	3	<i>f</i>	55.8656 (1.0-04)	...
0	0	10	2	<i>e</i>	0	0	9	3	<i>e</i>	61.0350 (1.4-02)	61.1361
2	2	0	3	<i>e</i>	0	0	9	2	<i>e</i>	61.7449 (5.5-03)	...
2	2	0	3	<i>e</i>	1	1	7	3	<i>f</i>	79.8265 (5.5-04)	...
0	0	10	1	<i>e</i>	0	0	9	2	<i>e</i>	90.7303 (1.5-02)	...
1	1	7	4	<i>e</i>	2	2	1	5	<i>e</i>	97.4626 (1.6-03)	...
0	0	10	0	<i>e</i>	0	0	9	1	<i>e</i>	111.7793 (4.1-02)	...
0	0	10	2	<i>e</i>	0	0	9	1	<i>e</i>	124.4950 (1.0-03)	...
1	0	2	5	<i>f</i>	2	2	1	5	<i>e</i>	125.0304 (1.6-04)	...
0	0	11	0	<i>e</i>	0	0	9	1	<i>e</i>	129.3389 (8.8-04)	...
0	0	10	1	<i>e</i>	0	0	9	0	<i>e</i>	129.4795 (1.4-02)	...

TABLE IX. Calculated transition frequencies (in GHz) for the morphed SH0 potential.

Upper state					Lower state					Frequency (GHz)	
$J_a$	$ \Omega $	$v$	$J$	$e/f$	$J_a$	$ \Omega $	$v$	$J$	$e/f$	Calc. (Int.)	Obs.
2	2	0	3	<i>e</i>	2	2	0	3	<i>f</i>	1.3057 (2.3-01)	...
0	0	10	1	<i>e</i>	0	0	10	0	<i>e</i>	4.7098 (4.0+00)	...
0	0	10	2	<i>e</i>	0	0	10	1	<i>e</i>	8.2736 (1.1+00)	...
2	2	0	3	<i>e</i>	1	1	7	4	<i>e</i>	9.9439 (8.7-04)	...
0	0	9	1	<i>e</i>	0	0	9	0	<i>e</i>	13.1203 (1.4+00)	...
0	0	11	0	<i>e</i>	0	0	10	1	<i>e</i>	13.6225 (8.5-02)	...
1	1	7	4	<i>e</i>	0	0	9	3	<i>e</i>	13.8542 (5.3-02)	...
2	2	0	3	<i>f</i>	0	0	9	3	<i>e</i>	22.4923 (3.6-03)	22.4842
0	0	9	2	<i>e</i>	0	0	9	1	<i>e</i>	25.7087 (3.5-01)	...
0	0	9	4	<i>e</i>	2	2	0	3	<i>e</i>	37.3756 (4.1-04)	...
0	0	9	3	<i>e</i>	0	0	9	2	<i>e</i>	37.4136 (2.0-01)	38.5031
0	0	10	2	<i>e</i>	2	2	0	3	<i>e</i>	40.7780 (6.2-04)	...
0	0	9	4	<i>e</i>	0	0	9	3	<i>e</i>	61.1737 (9.6-02)	61.1361
2	2	0	3	<i>e</i>	0	0	9	2	<i>e</i>	61.2117 (4.3-03)	...
0	0	10	2	<i>e</i>	0	0	9	3	<i>e</i>	64.5761 (1.3-02)	...
0	0	9	3	<i>e</i>	1	1	7	3	<i>f</i>	70.2012 (5.7-04)	...
0	0	10	1	<i>e</i>	0	0	9	2	<i>e</i>	93.7161 (1.5-02)	...
2	2	0	3	<i>e</i>	1	1	7	3	<i>f</i>	93.9992 (7.8-04)	...
0	0	10	0	<i>e</i>	0	0	9	1	<i>e</i>	114.7150 (4.1-02)	...
0	0	10	2	<i>e</i>	0	0	9	1	<i>e</i>	127.6984 (1.1-03)	...
0	0	10	1	<i>e</i>	0	0	9	0	<i>e</i>	132.5450 (1.4-02)	...
0	0	11	0	<i>e</i>	0	0	9	1	<i>e</i>	133.0473 (9.1-04)	...

The  $J_a=2, \Omega=0$  states below the  ${}^3P_1$  threshold are several orders of magnitude wider, because they can predissociate by direct potential coupling.

There is no plausible assignment for the isolated 31.5 GHz transition in the vicinity of the  ${}^3P_0$  threshold. It is just possible that it involves levels immediately below the  ${}^3P_2$  threshold, but this is not likely because all of them are quasi-bound. The narrowest such level in Table XI has a width of 7 MHz, and most of the others are much wider, so it is unlikely either that a sharp transition would be observed or

that molecules in the initial state would survive long enough to enter the detection region of the spectrometer. It seems more likely that the 31.5 GHz transition originates from a bound-bound ( $f \leftrightarrow f, \Delta J = \pm 1$ ) or bound-quasi-bound ( $f \leftrightarrow e, \Delta J = 0$ ) transition involving levels below the  ${}^3P_1$  threshold. There are several candidates at plausible frequen-

TABLE X. Energies and widths of levels lying just below the  $N^+ ({}^3P_1)$  threshold, calculated on the morphed SH1 potential. Levels of *f* symmetry are bound in this region, so no width is given for them.

$J$	$J_a$	$R$	$e/f$	$E$ (cm $^{-1}$ )	$\Gamma$ (cm $^{-1}$ )
0	2	2	<i>e</i>	46.0384	2.9897
0	1	1	<i>f</i>	47.8756	...
1	2	3	<i>e</i>	46.6014	2.8209
1	1	0	<i>f</i>	47.7872	...
1	1	1	<i>e</i>	47.9936	0.0041
1	1	2	<i>f</i>	48.2498	...
1	1	0	<i>f</i>	48.7188	...
2	2	4	<i>e</i>	47.7745	3.1059
2	1	1	<i>f</i>	47.9868	...
2	1	2	<i>e</i>	48.3310	0.0040
2	1	3	<i>f</i>	48.6801	...
3	1	3	<i>e</i>	45.0797	0.0463
3	1	4	<i>f</i>	46.1318	...
3	1	2	<i>f</i>	48.3397	...
3	1	3	<i>e</i>	48.7402	0.0017
4	1	3	<i>f</i>	45.0935	...
4	1	4	<i>e</i>	46.6600	0.0826
4	1	5	<i>f</i>	47.8741	...
5	1	4	<i>f</i>	46.7131	...
5	1	5	<i>e</i>	48.3693	0.1057

TABLE XI. Energies and widths of levels lying just below the  $N^+ ({}^3P_2)$  threshold, calculated on the morphed SH1 potential.

$J$	$J_a$	$R$	$e/f$	$E$ (cm $^{-1}$ )	$\Gamma$ (cm $^{-1}$ )
0	2	2	<i>e</i>	129.3455	0.1124
0	2	2	<i>e</i>	130.7950	0.0173
1	2	1	<i>e</i>	129.1142	0.0624
1	2	2	<i>f</i>	129.7485	0.0005
1	2	3	<i>e</i>	130.1736	0.0470
1	2	1	<i>e</i>	130.7343	0.0027
2	2	0	<i>e</i>	129.1147	0.0455
2	2	1	<i>f</i>	129.7602	0.0010
2	2	2	<i>e</i>	130.0851	0.0160
2	2	3	<i>f</i>	130.4585	0.0007
2	2	0	<i>e</i>	130.7106	0.0045
3	2	4	<i>f</i>	127.0334	0.0048
3	2	5	<i>e</i>	127.9447	0.1734
3	2	1	<i>e</i>	129.3744	0.0318
3	2	2	<i>f</i>	130.1351	0.0020
3	2	3	<i>e</i>	130.5764	0.0151
3	2	1	<i>e</i>	130.7663	0.0002
4	2	4	<i>e</i>	127.4085	0.1383
4	2	5	<i>f</i>	129.0025	0.0105
4	2	2	<i>e</i>	129.8326	0.0658
4	2	6	<i>e</i>	130.2619	0.1742
4	2	3	<i>f</i>	130.6417	0.0022
5	2	4	<i>f</i>	127.4527	0.0438
5	2	5	<i>e</i>	129.3134	0.1368
5	2	3	<i>e</i>	130.4711	0.0196
5	2	6	<i>f</i>	130.9322	0.0232

cies, such as that between the  $(J, J_a, R) = (4, 1, 3)$  level at  $45.09 \text{ cm}^{-1}$  and the  $(3, 1, 4)$  level at  $46.13 \text{ cm}^{-1}$ . The observation of a large hyperfine splitting in the 31.5 GHz transition suggests that at least one of the levels has considerable  $J_a = 2$  character. This is conceivable even for levels labeled  $J_a = 1$  because the potential can couple  $J_a = 1$  and 2 for  $|\Omega| > 0$ . However, a more likely possibility is that some of the  $J_a = 2$ ,  $|\Omega| = 1$   $f$  levels actually lie just below rather than just above the  ${}^3P_1$  threshold, and that the 31.5 GHz transition involves one of them.

## V. CONCLUSIONS

We have used the near-dissociation microwave rovibronic spectra of Carrington and co-workers<sup>6,15</sup> to obtain coupled potential energy curves for HeN<sup>+</sup> and to analyze the behavior of its energy levels near dissociation. We have carried out high-level *ab initio* calculations at the RCCSD(T) level, and then adjusted the curves slightly to fit the experimental frequencies. We have carried out fully coupled calculations of both bound and quasibound states lying near the N<sup>+</sup>  ${}^3P_0$ ,  ${}^3P_1$ , and  ${}^3P_2$  thresholds. All the quasibound states are found to have widths large enough that they would have caused observable broadening in the experimental lines.

We assign the main group of transitions, which have been shown by double resonance to share a common central level, to bound-state levels lying just below the N<sup>+</sup> ( ${}^3P_0$ ) threshold. There are two assignments that reproduce the experimental frequencies satisfactorily, but one of them (designated SH1) is preferred because it explains the lack of hyperfine splitting in the 61.1 GHz line.

The levels of HeN<sup>+</sup> just below the  ${}^3P_0$  dissociation threshold are qualitatively described by Hund's case (c), in which the N<sup>+</sup> atomic angular momentum  $J_a$  and its projection  $\Omega$  onto the internuclear axis are nearly conserved. Nevertheless, there are significant rotational couplings, which drive a transition towards Hund's case (e) and cause large parity doublings in the case (c) levels. For levels immediately below the  ${}^3P_1$  threshold, the level pattern is more satisfactorily described with case (e) quantum numbers.

## ACKNOWLEDGMENTS

We are grateful to the EPSRC for funding a Research Associateship for P.S. under Grant No. GR/L86968/01, and for the award of computer time at the Rutherford Appleton Laboratories, which enabled the *ab initio* part of these calculations to be performed. J.M.H. thanks JILA (University of Colorado and National Institute of Standards and Technology) for hospitality during his Visiting Fellowship in 2001-02. We are grateful to Professor R. J. Buenker and Dr. J.-P. Gu for providing details of their calculated potential energy curves, and to Dr. Lydia Heck and Dr. Joanna M. M. Howson for computational assistance.

- <sup>1</sup>W. C. Stwalley and H. Wang, *J. Mol. Spectrosc.* **195**, 194 (1999).
- <sup>2</sup>R. Wynar, R. S. Freeland, D. J. Han, C. Ryu, and D. J. Heinzen, *Science* **287**, 1016 (2000).
- <sup>3</sup>A. Carrington, C. A. Leach, A. J. Marr, A. M. Shaw, M. R. Viant, J. M. Hutson, and M. M. Law, *J. Chem. Phys.* **102**, 2379 (1995).
- <sup>4</sup>A. Carrington, C. H. Pyne, A. M. Shaw, S. M. Taylor, J. M. Hutson, and M. M. Law, *J. Chem. Phys.* **105**, 8602 (1996).
- <sup>5</sup>A. Carrington, D. I. Gammie, J. C. Page, A. M. Shaw, and J. M. Hutson, *J. Chem. Phys.* **116**, 3662 (2002).
- <sup>6</sup>A. Carrington, D. I. Gammie, A. M. Shaw, and S. M. Taylor, *Chem. Phys. Lett.* **262**, 598 (1996).
- <sup>7</sup>M. Meuwly and J. M. Hutson, *J. Chem. Phys.* **110**, 8338 (1999).
- <sup>8</sup>J. M. Bowman and B. Gazdy, *J. Chem. Phys.* **94**, 816 (1991).
- <sup>9</sup>B. Gazdy and J. M. Bowman, *J. Chem. Phys.* **95**, 6309 (1991).
- <sup>10</sup>J. M. Bowman and B. Gazdy, *Chem. Phys. Lett.* **200**, 311 (1992).
- <sup>11</sup>J. M. Bowman and J. Qi, in *Fashioning a Model: Optimization Methods in Chemical Physics*, edited by A. Ernesti, J. M. Hutson, and N. J. Wright (CCP6, Daresbury, 1998), p. 24.
- <sup>12</sup>A. L. Cooksy, D. C. Hovde, and R. J. Saykally, *J. Chem. Phys.* **84**, 6101 (1986); **89**, 5968(E) (1988).
- <sup>13</sup>J. M. Brown, T. D. Varberg, K. M. Evenson, and A. L. Cooksy, *Astrophys. J.* **428**, L37 (1994).
- <sup>14</sup>J. M. Brown, J. T. Hougen, K.-P. Huber, J. W. C. Johns, I. Kopp, H. Lefebvre-Brion, A. J. Merer, D. A. Ramsay, J. Rostas, and R. N. Zare, *J. Mol. Spectrosc.* **55**, 500 (1975).
- <sup>15</sup>D. I. Gammie, Ph.D. thesis, University of Southampton, 1999.
- <sup>16</sup>P. J. Knowles, C. Hampel, and H.-J. Werner, *J. Chem. Phys.* **99**, 5219 (1993); **112**, 3106(E) (2000).
- <sup>17</sup>J. Čížek, *J. Chem. Phys.* **45**, 4526 (1966).
- <sup>18</sup>D. E. Woon and T. H. Dunning, Jr., *J. Chem. Phys.* **100**, 2975 (1994).
- <sup>19</sup>S. F. Boys and F. Bernardi, *Mol. Phys.* **19**, 553 (1970).
- <sup>20</sup>MOLPRO is a package of *ab initio* programs written by H.-J. Werner and P. J. Knowles with contributions from others; for more information see the www page <http://www.tc.bham.ac.uk/molpro/>.
- <sup>21</sup>T.-S. Ho and H. Rabitz, *J. Chem. Phys.* **104**, 2584 (1996).
- <sup>22</sup>T. Hollebeck, T.-S. Ho, and H. Rabitz, *Annu. Rev. Phys. Chem.* **50**, 537 (1999).
- <sup>23</sup>P. Soldán and J. M. Hutson, *J. Chem. Phys.* **112**, 4415 (2000).
- <sup>24</sup>D. L. Cooper and S. Wilson, *Mol. Phys.* **44**, 161 (1981).
- <sup>25</sup>G. Frenking, W. Koch, D. Cremer, J. Gauss, and J. F. Liebman, *J. Phys. Chem.* **93**, 3397 (1989).
- <sup>26</sup>J.-P. Gu, R. J. Buenker, and G. Hirsch, *J. Chem. Phys.* **102**, 7540 (1995).
- <sup>27</sup>R. J. Buenker and J.-P. Gu (unpublished results).
- <sup>28</sup>R. S. Mulliken, *Rev. Mod. Phys.* **2**, 60 (1930).
- <sup>29</sup>J. M. Hutson, *Comput. Phys. Commun.* **84**, 1 (1994).
- <sup>30</sup>J. M. Hutson, BOUND computer program, version 6 (1993), distributed by Collaborative Computational Project No. 6 of the UK Science and Engineering Research Council.
- <sup>31</sup>D. E. Manolopoulos, Ph.D. thesis, University of Cambridge, 1988.
- <sup>32</sup>C. J. Ashton, M. S. Child, and J. M. Hutson, *J. Chem. Phys.* **78**, 4025 (1983).
- <sup>33</sup>J. M. Hutson and S. Green, MOLSCAT computer program, version 14 (1994), distributed by Collaborative Computational Project No. 6 of the UK Science and Engineering Research Council.
- <sup>34</sup>A. U. Hazi, *Phys. Rev. A* **19**, 920 (1979).
- <sup>35</sup>J. M. Hutson and C. J. Ashton, RESFIT computer program (1982).
- <sup>36</sup>R. J. Le Roy, LEVEL 7.1, a computer program for solving the radial Schrödinger equation for bound and quasibound levels, University of Waterloo Chemical Physics Research Report CP-642 R, 2000.
- <sup>37</sup>M. M. Law and J. M. Hutson, *Comput. Phys. Commun.* **102**, 252 (1997).